



**Numerical Simulation of
Radiation-Driven Targets for Light
Ion Inertial Confinement Fusion**

R.E. Olson, J.J. MacFarlane

April 1997

UWFDM-1045

Submitted to *Laser and Particle Beams*.

FUSION TECHNOLOGY INSTITUTE

UNIVERSITY OF WISCONSIN

MADISON WISCONSIN

DISCLAIMER

This report was prepared as an account of work sponsored by an agency of the United States Government. Neither the United States Government, nor any agency thereof, nor any of their employees, makes any warranty, express or implied, or assumes any legal liability or responsibility for the accuracy, completeness, or usefulness of any information, apparatus, product, or process disclosed, or represents that its use would not infringe privately owned rights. Reference herein to any specific commercial product, process, or service by trade name, trademark, manufacturer, or otherwise, does not necessarily constitute or imply its endorsement, recommendation, or favoring by the United States Government or any agency thereof. The views and opinions of authors expressed herein do not necessarily state or reflect those of the United States Government or any agency thereof.

Numerical Simulation of Radiation-Driven Targets for Light Ion Inertial Confinement Fusion

R. E. Olson

Sandia National Laboratories
Albuquerque, NM 87185

J. J. MacFarlane

Fusion Technology Institute
University of Wisconsin
Madison, WI 53706

Light ion beam inertial confinement fusion (ICF) is a concept in which intense beams of low atomic number ions would be used to drive ICF targets to ignition and gain. Here, results from numerical simulations are presented describing the operation of an indirect-drive light ion inertial confinement fusion (ICF) target designed for an commercial power plant application. The simulations indicate that the ICF target, consisting of an x-ray driven capsule embedded in a spherical foam-filled hohlraum, will produce a fusion energy output of over 500 MJ when driven with lithium ion beams containing a total input energy of 8 MJ.

1. Background and introduction

The concept of using light ion beams to compress matter to the densities required for high gain ICF has been an area of active research for about 20 years. Yonas (1978) wrote one of the first review articles on this subject. An overview of recent progress was provided by Quintenz et al. (1996). Although some early work involved directly-driven ICF targets (e.g., Clauser 1975), the main approach to light ion ICF since the late 1970's has been based upon indirect-drive. In indirect drive ICF, the driver energy is absorbed in a high-Z enclosure (or "hohlraum") that surrounds a spherical shell (or "capsule") containing DT fuel. The hohlraum is heated by the driver and the interior walls emit x-rays, which are absorbed

by the capsule material (the "ablator") and drive the implosion. In the ion-driven version of this concept, the capsule is embedded within a spherical foam-filled hohlraum (Figure 1). The high energy ions penetrate the hohlraum wall and deposit the bulk of their energy in a low-density CH foam, which converts the ion beam energy into soft x-rays that have a high enough energy to freely traverse the ionized CH plasma, but are trapped by the high opacity hohlraum wall. This "greenhouse target" indirect-drive ICF concept was first discussed in internal Sandia reports in the late 1970's and early 1980's. Slutz (1979) described the basic concept and provided analytic estimates of target performance. Allshouse (1981) provided numerous detailed computational simulations of ion-driven greenhouse target performance. Overviews of an experimental program in which this type of ion-driven hohlraum has been demonstrated can be found in Leeper et al. (1995) and Quintenz et al. (1996). A description of an ion-driven ICF target designed for defense applications, together with a conceptual design of a light ion beam driver for such a target -- the Laboratory Microfusion Facility (LMF) -- was provided by Olson et al. (1993).

Over the last ten years, light ion ICF energy applications have been studied in a series of electrical power plant conceptual designs referred to as LIBRA (Light Ion Beam ReActor). Moses et al. (1989) and Kulcinski et al. (1994) have published descriptions of the LIBRA power plant studies (Figure 2). In the present paper, we describe numerical simulations of the implosion and burn of an indirectly-driven ICF target designed specifically for the LIBRA power plant parameters. Numerical simulations of the explosion dynamics and energy release of this target in a LIBRA reactor chamber are the subject of a companion paper by MacFarlane et al. (1996).

In any electrical power plant concept, part of the thermonuclear output must be recycled back to the driver. Thus, as pointed out by Nuckolls et al. (1972) and detailed by Bodner (1981), there is a requirement on target "gain" (\equiv thermonuclear energy output/driver energy on target) that will depend upon details of electrical conversion efficiency, driver efficiency, etc. These many details are the subject of the LIBRA studies which indicate that an economical light ion power plant must have a target gain > 60 . To achieve such a gain, the majority of the DT fuel must be compressed at a cold temperature (nearly Fermi-degenerate) with only a small, central portion of the fuel heated by driver energy to ignition-level temperatures. This type of compression can be achieved via a controlled increase in shock pressure ("pulse shaping") as the implosion proceeds (Nuckolls et al., 1972). The energy output from the central hot spot heats the cold, compressed DT via a propagating burn. Thus, for high gain, the imploded DT fuel at time of ignition should

have a high temperature hot spot with a density-radius product (ρr) sufficient for ignition surrounded by a cold, high density main fuel region. To successfully arrive at this fuel configuration, the pulse-shaped capsule implosion must satisfy some basic requirements related to symmetry, stability, ignition, and burn (Lindl 1995). Our goal in this work is to provide a LIBRA target concept that, in numerical simulations of the capsule implosion, provides a gain of 60 while adhering to the known limitations on symmetry, stability, and pulse shape.

2. Physics models

Our simulations of the ion deposition, radiation transport, capsule implosion, and fusion burn of the LIBRA target have been performed with the 1-D radiation hydrodynamics computer code BUCKY-1 (MacFarlane et al. 1995). The BUCKY-1 code, which is a descendant of the PHD-IV code (Moses et al. 1985), is a 1-D Lagrangian code which solves the single-fluid equations of motion with pressure contributions from electrons, ions, radiation, and fast charged particle reaction products. Ion beam deposition is calculated via the finite material temperature ion energy deposition model of Mehlhorn (1981). Energy transfer in the plasma is treated with a two temperature model -- separate ion and electron temperatures. Thermal conduction through each species is treated using Spitzer's form of thermal conductivity. The electron conductivity is flux limited. Radiation emission and absorption terms couple the electron temperature equation to the radiation transport equations. In addition, the electron and ion temperature equations contain source terms that couple them to the ion beam energy deposition calculation and the energy deposited from the fusion reactions. The fusion reaction products are transported and slowed using a time-dependent particle tracking algorithm.

In the simulations described below, SESAME equations of state (Lyon & Johnson 1992) were used, and multigroup opacities were generated with the EOSOPA code (Wang 1993). EOSOPA includes opacity contributions from bound-bound and free-free transitions. It utilizes a detailed term accounting (DTA) model for low-Z atomic systems and an unresolved transition array (UTA) model for high-Z systems. Radiation transport is calculated using a diffusion model with 100 frequency groups. The time-dependent radiation energy density equations are solved using finite difference techniques.

Since our numerical simulations are 1-D, we must be careful to include constraints related to implosion symmetry, which is multidimensional in nature. For symmetry

constraints, we rely on numerical simulations previously performed for a similar light ion ICF target designed for the aforementioned defense applications LMF proposal. In that work (Allshouse et al. 1993), a three dimensional ion deposition code and a three dimensional deterministic radiation transport code were used to determine the effects of ion deposition nonuniformities on the x-ray uniformity at the capsule (including time and temperature dependent effects such as range shortening and hydrodynamic motion). This information was then coupled with two dimensional implosion and fusion burn simulations using the LASNEX radiation hydrodynamics code (Zimmerman & Kruer, 1975). The LMF calculations indicated that an illumination scheme involving a 2 cm diameter hohlraum and twelve individual ion beams with a 1.2 cm fwhm rotationally-symmetric Gaussian distribution would provide an adequately symmetric x-ray drive for an LMF target having a hohlraum radius / capsule radius ratio of 4:1 and a hot spot convergence ratio of 25:1 (Olson, 1993). Since the LIBRA electrical power plant also proposes using a 12 beam illumination scheme, we limit our LIBRA calculations to have hohlraum radius / capsule radius and hot spot convergence ratios of a similar magnitude.

Perturbation growth rates and mixing due to Rayleigh-Taylor fluid instability are also important issues that are not directly addressed in our 1-D BUCKY calculations. Limitations on the degree of mixing of hot and cold DT due to hydrodynamic instabilities is thought to be crucial to the successful formation of the central hot spot. Lindl (1995) points out that the peak magnitude of the in-flight aspect ratio (IFAR) -- which is defined as the ratio of the capsule shell radius to its thickness as it implodes -- can be used to estimate whether or not the instability growth (assuming some realistic capsule surface finish) will result in an intolerable degree of mixing during hot spot formation. Thus, to account for instability and mix constraints, we put limits on the acceptable peak IFAR in our 1-D BUCKY simulations of LIBRA targets.

3. Numerical simulations of the capsule implosion

The LIBRA indirect drive target is shown in Figure 3. The capsule consists of a spherical polycarbonate ($C_{16}H_{14}O_3$) shell that contains 5 mg of DT fuel. The capsule is initially at a cryogenic temperature, and we assume that a β -layering technique (Hoffer & Foreman 1988) is used to arrange the DT in a uniform solid layer on the inner surface of the polycarbonate shell. A DT vapor pressure consistent with the β -layering temperature of about 18 K provides a central, low density region of DT at 0.5 mg/cc. The $C_{16}H_{14}O_3$ shell has a 0.48 cm inner diameter and is 180 μm thick. This polycarbonate shell is, essentially, the x-ray driven ablator material. A 30 μm thick CF_2 coating on the outside of the shell is

used to assist in the pulse shaping of the implosion via an internal pulse shaping technique (Olson et al. 1996). The x-ray driven capsule is embedded in a low density (15 mg/cc) CH foam, and the foam is encased by a 1.4 cm diameter, 15 μm thick spherical Au shell.

The ion beam input power for the calculation is illustrated in Figure 4. The target is driven by a two-step lithium ion beam power pulse that is consistent with the LIBRA-SP driver concept (Kulcinski et al. 1994). A 30 TW input of 20 MeV lithium ions supplies power for 40 ns (the "foot" pulse) and an input of 480 TW of 30 MeV lithium ions drives the calculation for the last 14 ns (the "main power" pulse). Plots of ion power deposition vs. radius for times during the low power foot pulse are shown in Figure 5. The ions penetrate the Au zones and deposit the bulk of their energy in the zones making up the CH ion deposition region of the calculation. The inner low density CH region acts as an "isolation layer" which protects the capsule from a direct imprinting of ion beam asymmetries. This region is designed such that a supersonic radiation front outruns the local shocks so that the first shocks in the capsule are driven by the hohlraum radiation field. Plasma in the low density, low-Z ion deposition region volumetrically radiates x-ray power at a rate that approximately balances the local ion deposition power. The majority of this x-ray power is absorbed and then re-emitted by the inner Au plasma zones. The capsule is driven by a combination of x-rays emitted from the wall and from the foam. When the low-Z foam is hot (>70 eV), drive photons freely traverse the case-to-capsule distance, and the majority of the capsule drive originates at the high-Z hohlraum wall. This is possible due to the high albedo ($>80\%$) of the high-Z wall plasma. As is shown in Figure 6, the resulting radiation field is uniform throughout the low-Z plasma between the hohlraum wall and capsule ablator material. A plot of the hohlraum radiation temperature history is shown in Figure 7. This radiation field is essentially the "drive" for the ICF capsule.

Most of the x-ray power incident upon the capsule is absorbed and converted into kinetic energy (hydrodynamic motion of the ablator material). Early in time, during the foot power pulse, the ablation front is in the outer CF_2 region of the capsule. This ablation sets up a slow (~ 1 cm/ μs), low pressure (~ 1 Mbar) shock. After this initial shock traverses and compresses most of the DT layer, the pressure timing at the $\text{C}_{16}\text{H}_{14}\text{O}_3$ / DT interface is affected by the radiation absorption and ionization characteristics of the CF_2 plasma. As the CF_2 temperature increases, the corresponding capsule albedo decrease is nonmonotonic, due primarily to the changes in opacity that occur as the fluorine K-shell electrons are ionized. This nonmonotonic albedo change provides a pause in the rise of the

capsule drive even as the hohlraum temperature is increasing. This pause provides time for a second, ~5-10 MB shock to traverse the compressed DT layer. A little bit later in time, the ablation front leaves the CF_2 layer and enters the $\text{C}_{16}\text{H}_{14}\text{O}_3$ "main ablator" region. As shown in Figure 8, the ablation pressure increases rapidly (nearly doubling) when the ablation front enters the $\text{C}_{16}\text{H}_{14}\text{O}_3$. This rapid pressure increase compensates for the rarefaction wave that is in the process of returning from the DT solid/vapor interface. In the meantime, the drive as seen by the ablation front in the $\text{C}_{16}\text{H}_{14}\text{O}_3$ is filtered by the CF_2 plasma surrounding the capsule. Thus, we get a gradually increasing acceleration pressure caused by the increasing x-ray transmission due to fluorine inner shell ionization in the CF_2 blowoff plasma. At approximately 48 ns into the simulation, the fluorine becomes fully ionized and the main ablator experiences the full drive of the outer hohlraum environment. As shown in the radius vs. time plot of Figure 9, the ablation pressure increase provides a controlled acceleration and compression of the DT fuel with a peak IFAR of 48, a peak implosion velocity of 3×10^7 cm/s, and a hot spot convergence ratio of 18. The imploded fuel configuration (i.e., overlaid profiles of the ion temperature and DT density) just as the fusion burn is beginning to propagate is shown in Figure 10.

A summary of the entire DT compression, ignition, and thermonuclear burn process for this simulation can be seen in the Figure 11 plots of pressure vs. density for calculational zones in the dense DT region. It can be seen that the initial shock in the outer DT zones is 1 Mbar and compresses the DT from its initial density of 0.219 g/cm^3 to about 1 g/cm^3 . The shock breakout, rarefaction and recompression of the inner zones are evident in the figure. Subsequent shocks of ~5, 10, and 20 Mbars compress the bulk of imploding fuel (the outer zones) along a nearly Fermi-degenerate limiting energy density trajectory to a peak density of several hundred g/cm^3 . At the same time, it can be seen that the inner zones (which rapidly blow into the central region) are shock heated to a much higher temperature and then compressed to densities ~ 20-100 g/cm^3 . At this point, when the hot spot ρr exceeds ~ 0.25 g/cm^2 , the DT ignites and a sudden, almost constant density jump in pressure occurs as the burn wave propagates through the DT zones, providing a total thermonuclear yield of 520 MJ. Of the total yield, approximately 70% of the energy is carried away by neutrons; about 22% of the target yield is emitted in the form of x-rays; and the remainder is carried away in debris ion kinetic energy. Details of the emitted neutron and x-ray spectra and target debris explosion dynamics are presented in a companion paper by MacFarlane et al. (1996). As pointed out in that paper, detailed target yield predictions of this type provide an important input for the LIBRA reactor conceptual design activities.

4. Summary

We have performed 1-D numerical simulations of the implosion and burn of indirect-drive ICF targets designed for commercial power plant applications. For the LIBRA-SP target configuration presented here, our calculations predict a total thermonuclear yield of 520 MJ with a lithium ion beam input of 8 MJ. According to LIBRA calculations (Moses et al. 1989, Kulcinski et al. 1994), this target gain should be adequate to project an economically competitive light ion driven commercial power plant.

Acknowledgments

The authors thank P. Wang for generating the opacity tables used in these calculations. This work was supported by the U.S. Department of Energy under Contract No. DE-AC04-94AL85000.

REFERENCES

- ALLSHOUSE, G. O. 1981 Res. Rep. SNL.
- ALLSHOUSE, G. O. 1993 private communications.
- BODNER, S. E. 1981 Critical Elements of High Gain Laser Fusion, NRL Memorandum Rpt. 4453.
- CLAUSER, M. J. 1975 Phys. Rev. Lett. 35, 848.
- HOFFER, J. K. & FOREMAN, L. R. 1988 Phys. Rev. Lett. 60, 1310.
- KULCINSKI, G. L. 1994 Fusion Technology 26, 849.
- LEEPER, R. J. et al. 1995 J. Plasma & Fusion Research 71, 945.
- LINDL, J. 1995 Phys. Plasmas 2, 3933.
- LYON S. P. & JOHNSON, J. D., eds. 1992 SESAME: The Los Alamos National Laboratory Equation of State Database, LANL Report LA-UR-92-3407.
- MACFARLANE et al. 1995 BUCKY-1 -- A 1-D Radiation Hydrodynamics Code for Simulating Inertial Confinement Fusion High Energy Density Plasmas, Univ. of Wisconsin Fusion Tech. Inst. Rep. UWFDM-984.
- MACFARLANE, J. J. et al. 1996 Fusion Tech.
- MEHLHORN, T. A. 1981 J. Appl. Phys. 52 6522.
- MOSES, G. A. et al. 1985 A Plasma Hydrodynamics, Thermonuclear Burn, Radiative Transfer Computer Code, Univ. of Wisconsin Fusion Tech. Inst. Rep. UWFDM-194.
- MOSES, G. A. et al. 1989 Laser and Particle Beams 7, 721.

- NUCKOLLS, J et al. 1972 Nature 239, 139.
- OLSON, R. E. et al. 1993 Emerging Nuclear Energy Systems -- ICENES '93 -- Proc. 7th Int. Conf., Chiba, Japan, 91 (World Scientific Publishing, Singapore).
- OLSON, R. E. et al. 1994 Fusion Technology 26, 922.
- OLSON, R. E. et al. 1996 Phys. Plasmas.
- QUINTENZ, J. P. et al. 1996 Progress in Nuclear Energy 30, 183 (Elsevier Science Ltd.).
- SLUTZ, S. A. 1979 Res. Rep. SNL; also, 1995 Laser and Particle Beams 13,243.
- WANG, P. 1993 EOSOPA -- A Code for Computing the Equations of State and Opacities of High Temperature Plasmas with Detailed Atomic Models, University of Wisconsin Fusion Technology Institute Report UWFDM-933.
- YONAS, G. 1978 Sci. Am. 239, 50.
- ZIMMERMAN, G. B. & KRUEER, W. L. 1975 Comments Plasma Phys. 2, 51.

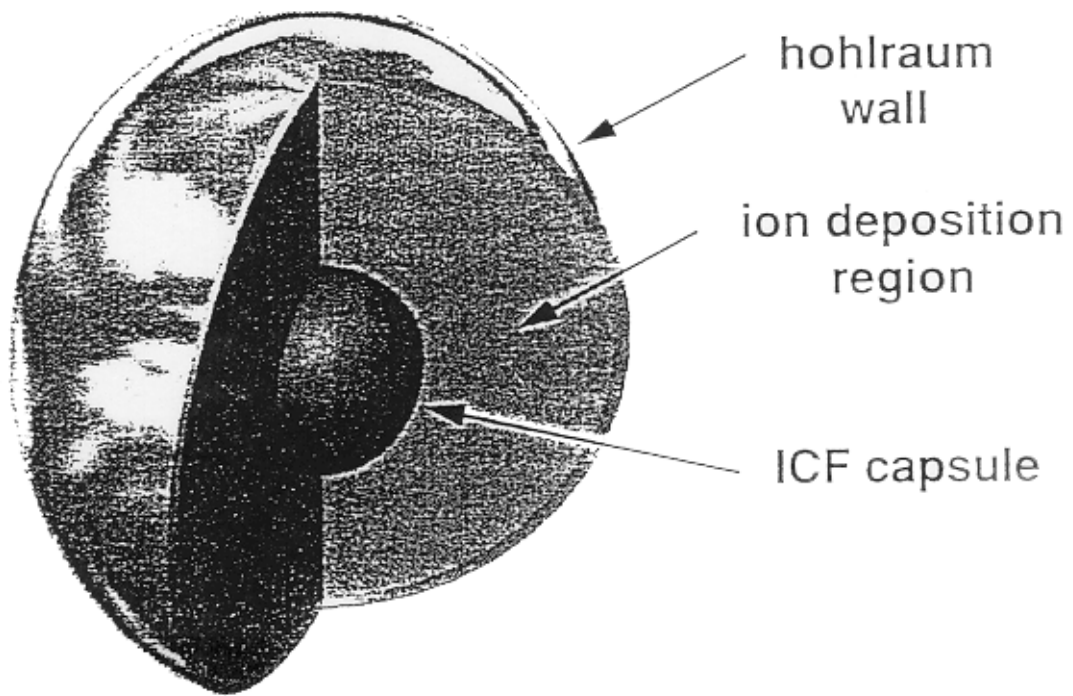
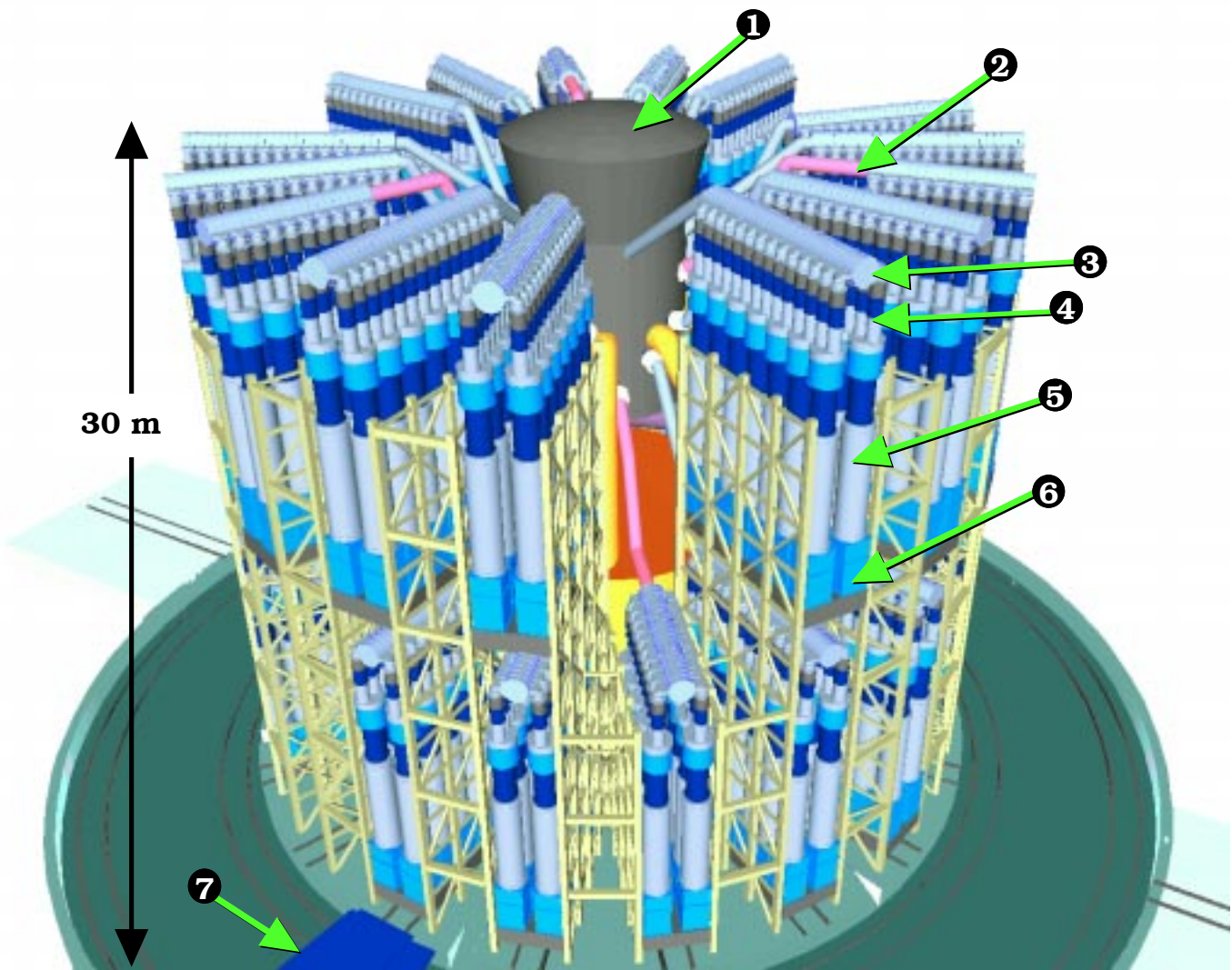


Figure 1. Basic configuration of an ion-driven ICF target.



(1) Reactor chamber

(2) Driver

(3) Adder cells

(4) Pulse forming lines

(5) 5 μs stage

(6) Capacitors and switches

(7) Transport carriage

Figure 2. Isometric view of the LIBRA reactor concept (from Kulcinski et al. 1994).

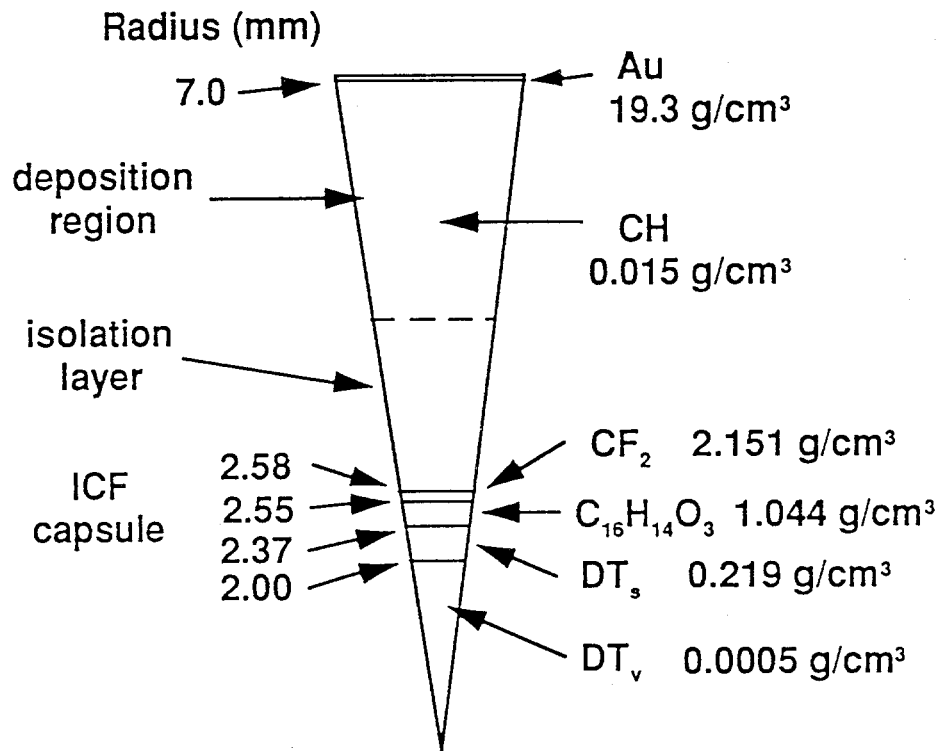


Figure 3. Dimensions of a light ion driven target having a predicted 520 MJ thermonuclear yield.

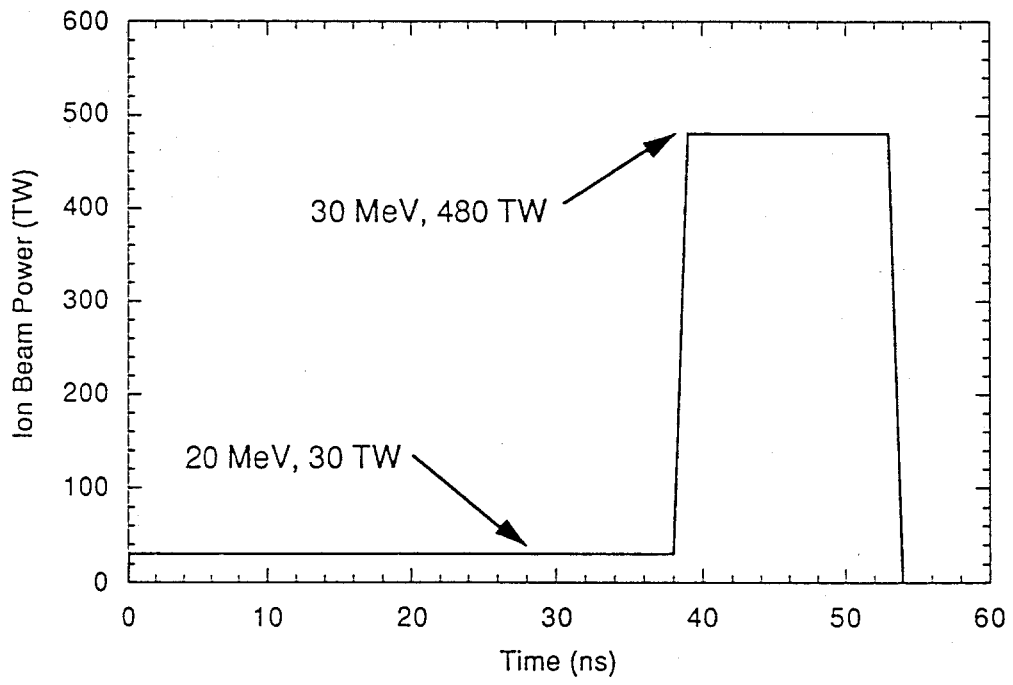


Figure 4. On-target ion beam power requirements for a predicted 520 MJ thermonuclear yield.

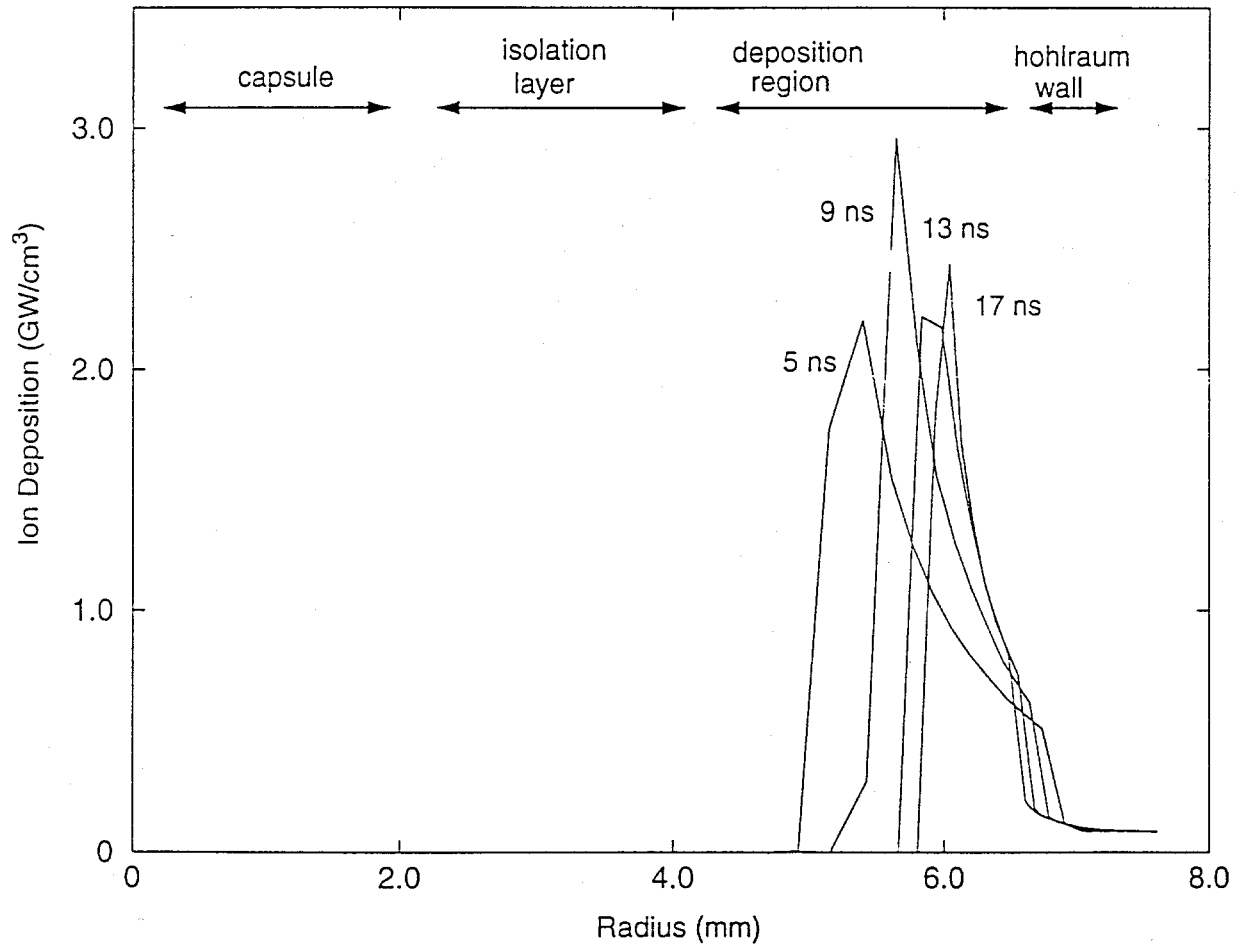


Figure 5. Ion beam power deposition rate (GW/cm³) as a function of radius (mm) at times during the low power phase of the ion beam drive.

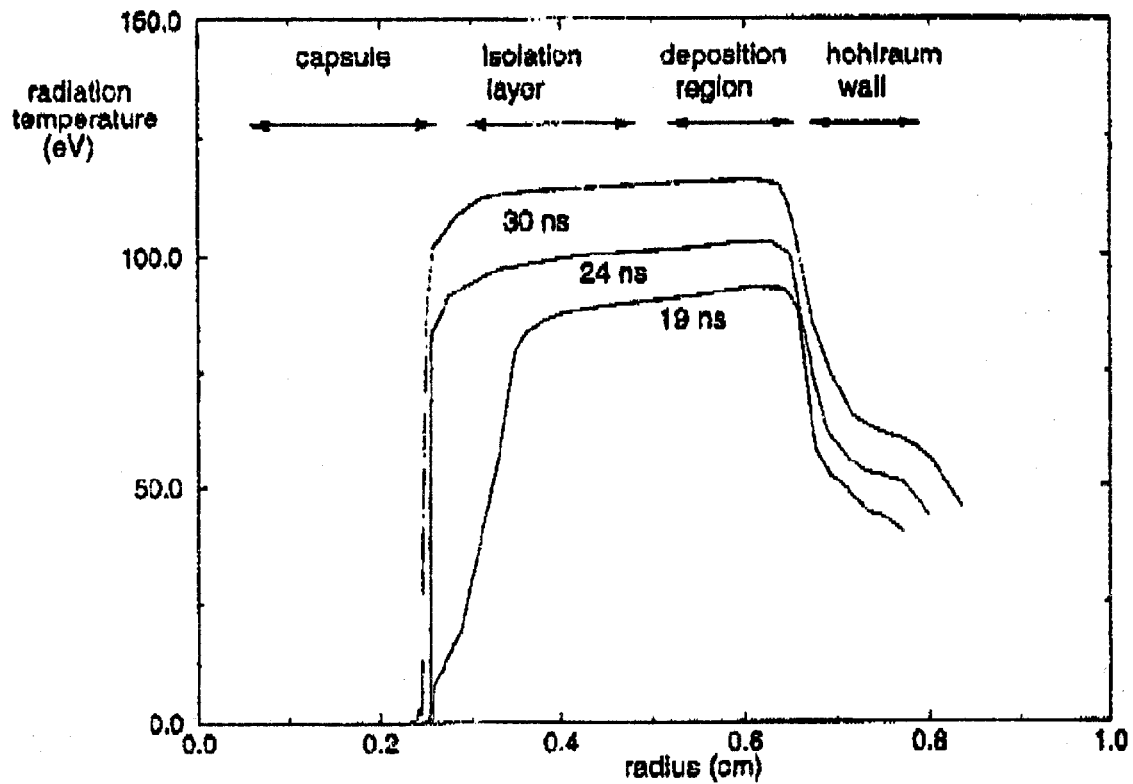


Figure 6. Radiation temperature (eV) as a function of radius (mm) during the lower power phase of the beam drive. Note that the radiation field is uniform throughout the low-Z plasma between the hohlraum wall and capsule ablator.

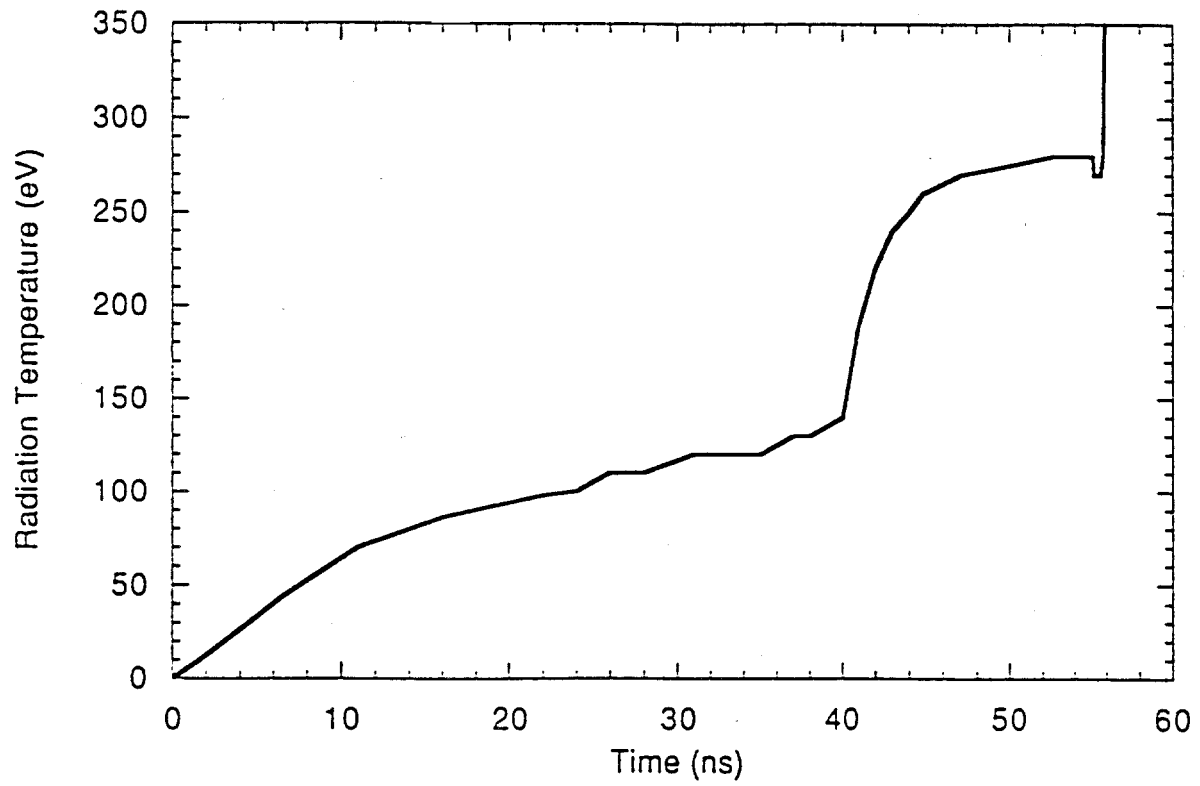


Figure 7. Hohlraum radiation temperature as a function of time.

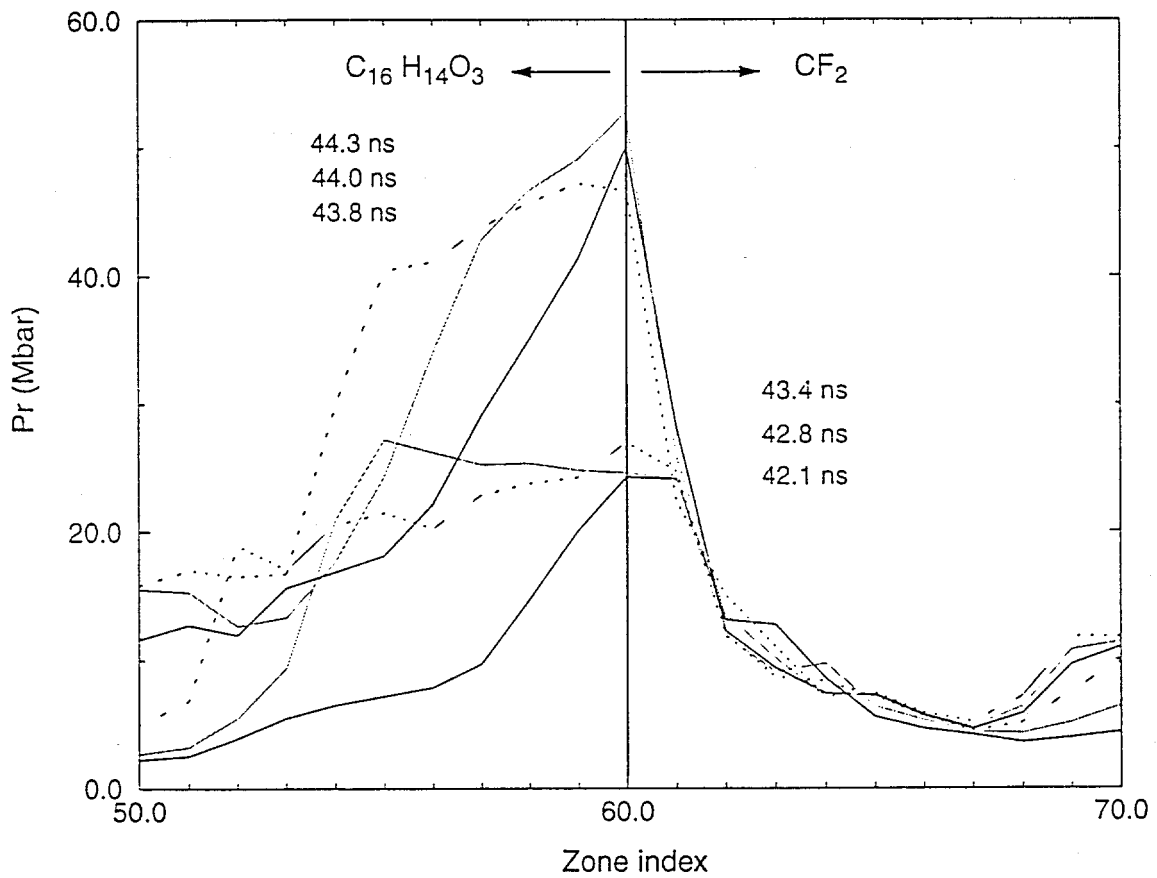


Figure 8. Shock pressure (Mbar) as a function of zone number at times during the compression and implosion process. Note the sudden jump in shock pressure as the ablation front moves from the CF_2 into the $C_{16}H_{14}O_3$.

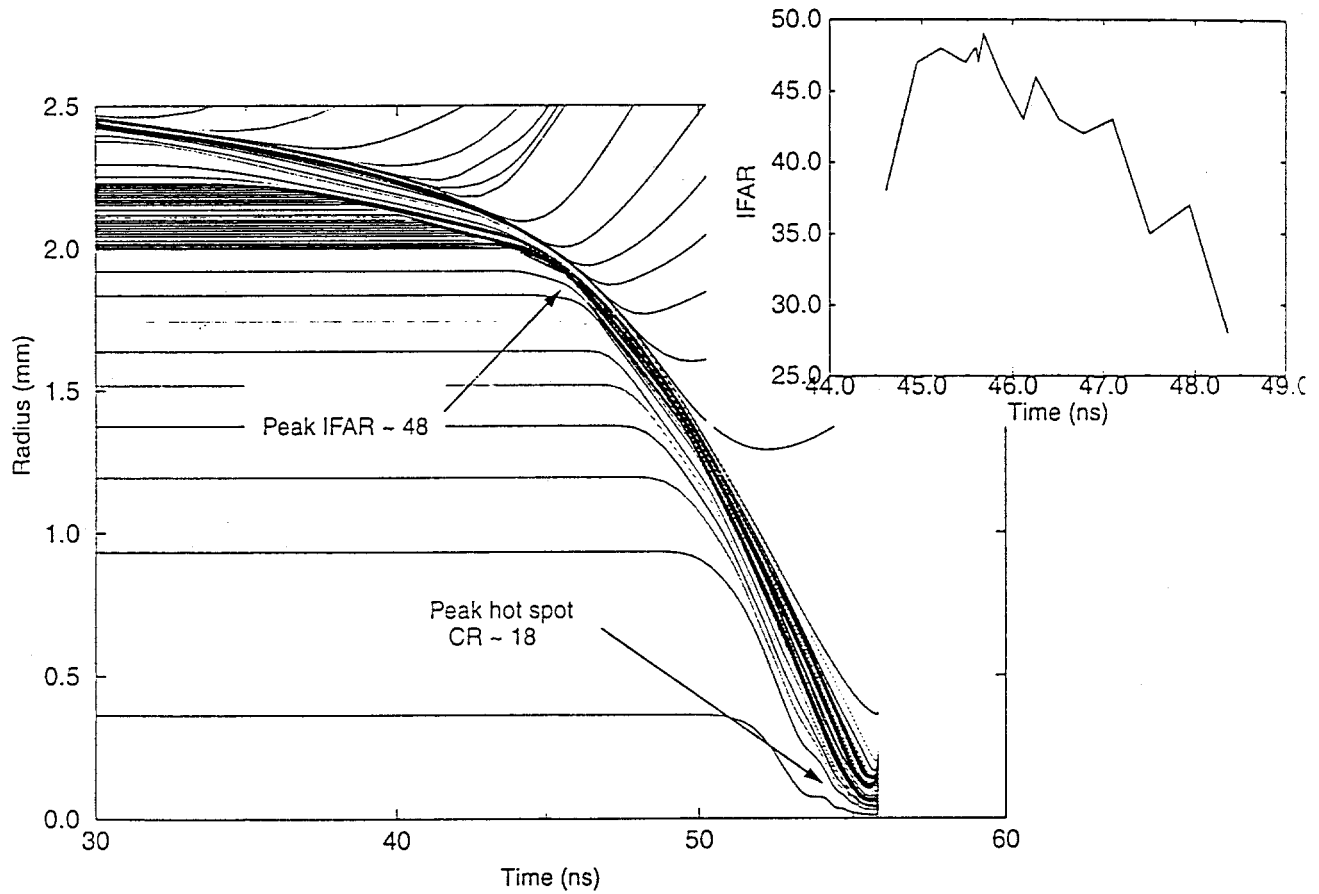


Figure 9. Zone radius (cm) as a function of time (ns) during the compression and implosion process. Inset is a plot of IFAR (1/e in-flight aspect ratio) as a function of time.

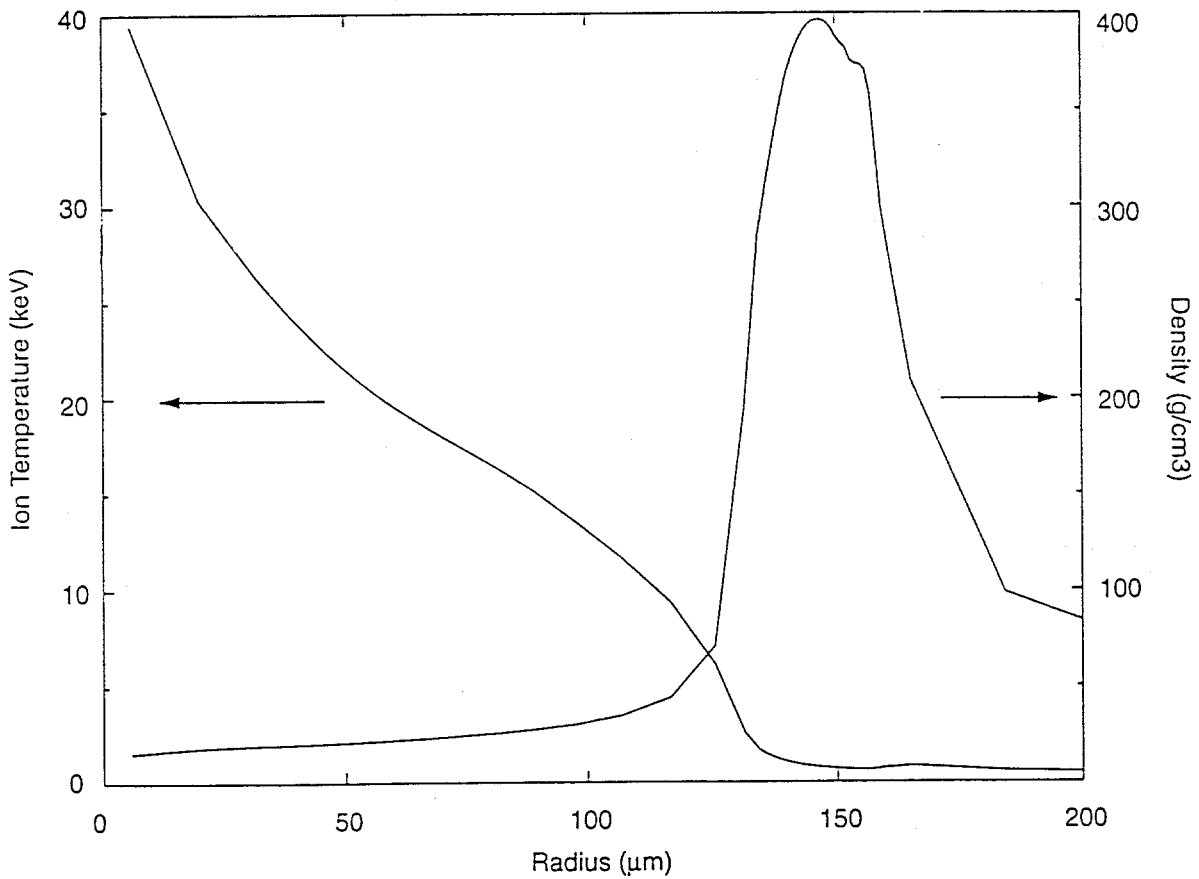


Figure 10. DT fuel density (g/cm^3) as a function of radius (mm) and ion temperature (keV) as a function of radius (mm) plotted as the thermonuclear burn is beginning to propagate through the dense DT region.

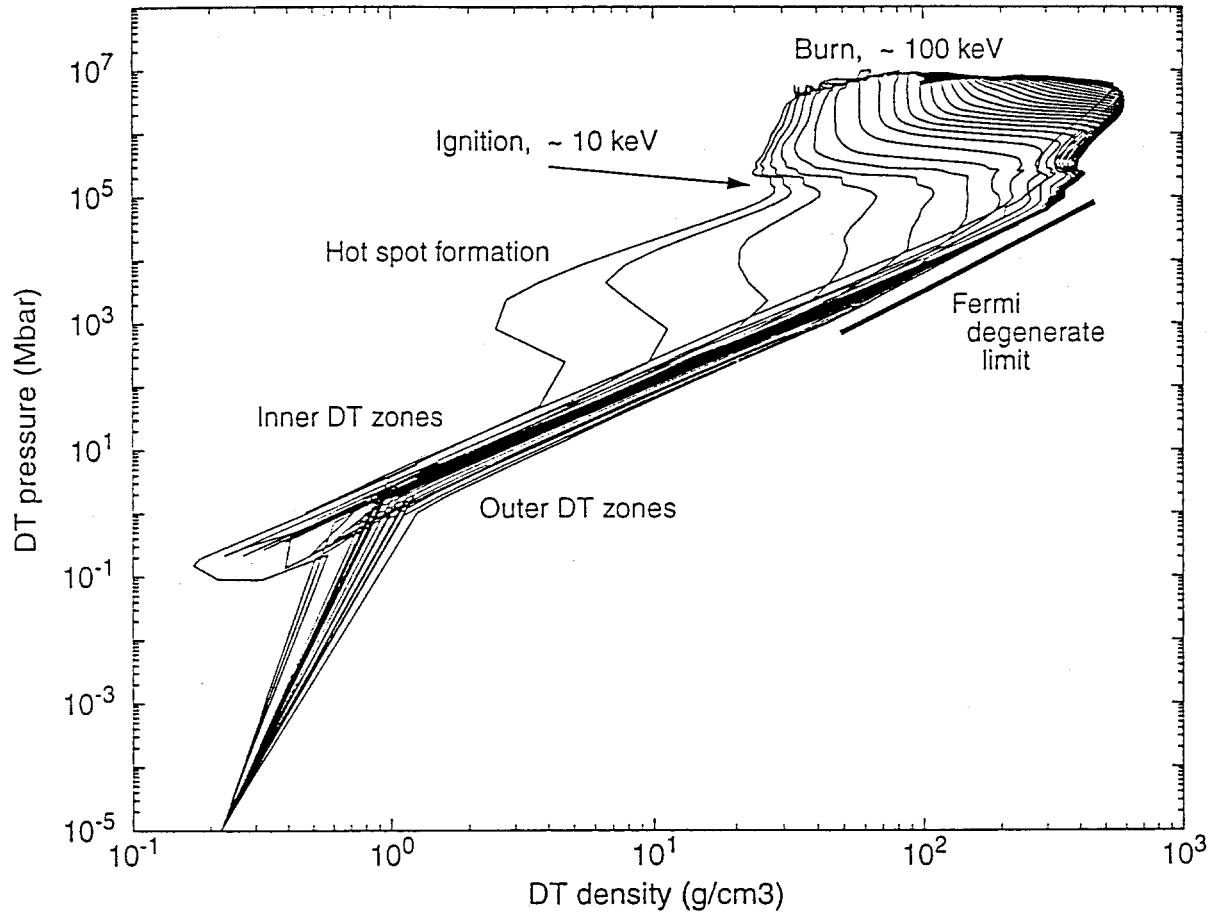


Figure 11. DT pressure (Mbar) as a function of DT density (g/cm^3) for zones in the DT region of the capsule. Note that most of the fuel is compressed with a nearly Fermi-degenerate minimum energy investment.